



ELSEVIER

Contents lists available at ScienceDirect

Inorganica Chimica Acta

journal homepage: www.elsevier.com/locate/ica

Research paper

 $[V^{IV}O]^{2+}$ complexes: Structure, unusual magnetic properties and cytotoxic effectL. Joshua Hernández-Benítez^a, Pamela Jiménez-Cruz^a, Karla E. Cureño-Hernández^a, Alejandro Solano-Peralta^b, Marcos Flores-Álamo^b, Angelina Flores-Parra^c, Isabel Gracia-Mora^d, Silvia E. Castillo-Blum^{a,*}^a Departamento de Química Inorgánica y Nuclear, Facultad de Química, Universidad Nacional Autónoma de México, Ciudad Universitaria, Coyoacán, CDMX 04510, México^b Unidad de Servicios de Apoyo a la Investigación y a la Industria, Facultad de Química, Universidad Nacional Autónoma de México, Ciudad Universitaria, Coyoacán, CDMX 04510, México^c Departamento de Química, Centro de Investigación y de Estudios Avanzados, AP 14-740, CDMX 07000, México^d Unidad de Investigación Preclínica, Facultad de Química, Universidad Nacional Autónoma de México, Ciudad Universitaria, Coyoacán, CDMX 04510, México

ARTICLE INFO

Keywords:

Cytotoxic activity
EPR spectroscopy
Magnetic properties
Oxidovanadium(IV) complexes
X-ray crystal structures

ABSTRACT

The present investigation was carried out with the aim of synthesizing and characterizing five vanadium coordination compounds (**6–10**) with different Schiff bases (**1** = N,N'-bis(salicylidene)-o-phenylenediamine, **2** = N,N'-bis(4-hydroxysalicylidene)-o-phenylenediamine, **3** = N,N'-bis(4-methoxysalicylidene)-o-phenylenediamine, **4** = N,N'-bis(3-hydroxysalicylidene)-o-phenylenediamine, **5** = N,N'-bis(3-methoxysalicylidene)-o-phenylenediamine) and studying their cytotoxic properties. Based on their physical (magnetic susceptibility), spectral (X-ray, electronic, IR, ¹H NMR, ¹³C NMR, EPR and mass) and analytical (elemental analysis) results, the structures of these Schiff bases and their respective oxidovanadium(IV) complexes were established. Crystal structures of compounds **6** (Monoclinic, C 2/c, Z = 16) and **7–8** (Triclinic, P-1, Z = 2) had been determined by X-ray diffraction and confirmed pentacoordination of vanadium(IV) with a slightly distorted square-pyramidal geometry. Vanadium coordination compounds displayed low effective magnetic moments (0.85–0.89 BM) that maybe due to the intermolecular hydrogen bonding and π -stacking interactions in the crystal arrangements. Cytotoxic activity was evaluated on human tumor cell lines: **6–9** (HeLa = 0.443–1.502 μ M) and **6–10** (HCT-15 = 0.373–1.415 μ M), with exception of **7**. Cell growth inhibition revealed that regardless of the cancer cell line type compounds **6** and **8** showed similar activity -possible effect due to the complex *per se*- giving new insights into the structure–activity relationship for these complexes.

1. Introduction

Vanadium is a well-known metal of high importance in physiology, environment and industry. It is a first-row transition metal with electronic configuration of $[Ar]3d^34s^2$ [1]. Its oxidation states span from –1 to +5, being +3, +4 and +5 the most common. Elemental vanadium does not occur in nature and $[V^{IV}O]^{2+}$ ion is the most stable [2]. The abundance of vanadium in the crust of the planet is relatively high (c.a. 0.019%) and is the same case in sea water, where it is the second transition metal more abundant; nevertheless, the interest on the research of vanadium coordination compounds before 1980 was scarce [3].

Vanadium coordination compounds may exhibit different biological effects going from diabetes and lipid profile regulation [4,5],

conflicting risks in hypertension and heart diseases to regulation of cancer and apoptosis [5].

It is found in vanadium-dependent haloperoxidases and alternative nitrogenases [1], its individual species show important effects inhibiting the function of many enzymes, e.g., phosphatases (protein tyrosine phosphatases) [5a–5d], phosphorylases (Na^+ , K^+ -ATPases, Ca^{2+} -ATPases [5a–5d]) and ribonucleases [5c] and stimulating the function of others, e.g., SOD (superoxide dismutase), CAT (catalase), GSH-Px (phospholipid hydroperoxide glutathione peroxidase) and Mn-SOD [5d]. Vanadium(V) is an analogue of phosphorus and thus an inhibitor against phosphorylases. Additionally, this metal shows toxicity in large amounts but it is considered by some authors to be an essential element for humans [6].

The metal based compounds such as vanadium, titanium, copper,

* Corresponding author.

E-mail address: blum@unam.mx (S.E. Castillo-Blum).

ruthenium, tin and rhodium have been reported as promising chemotherapeutic drugs [7]. In addition, vanadium coordination compounds have received considerable attention as antitumor agents against murine tumors (leukemia, Ehrlich ascites tumor and mammary adenocarcinoma) with insulin-like and antihyperlipidemic properties in human body [8].

The structural features of Schiff bases are of interest in coordination chemistry; these types of ligands have been used for the synthesis of complexes with transition metal ions. The complexes display properties which are useful for a wide range of applications, such as in pharmacology, catalysis and sensors [9,10]. It has already been reported that tetradentate Schiff bases such as *N,N'*-bis(salicylidene)-*o*-phenylenediamine readily form complexes with vanadium salts yielding oxido-vanadium complexes [10]. For these reasons, herein we report the synthesis, characterization and evaluation of the potential cytotoxic activity of five vanadium coordination compounds using Schiff bases as N_2O_2 donor group.

2. Experimental

2.1. Reagents and solvents

Chemicals were purchased from various commercial suppliers and were used without further purification. All differently substituted 3,4-salicylaldehydes, *o*-phenylenediamine, $VO(acac)_2$, propylene glycol, cisplatin and sulforhodamine B were obtained from Sigma-Aldrich and solvents used for the synthesis and purification from J.T. Baker.

2.2. Instrumentation

IR spectra in the range $4000\text{--}400\text{ cm}^{-1}$ were performed on a Perkin Elmer FTIR/FIR Spectrum 400 spectrophotometer with a universal ATR sampling accessory at room temperature. NMR spectra of the ligands were recorded on a Varian VNMRs (400 MHz) spectrometer in $DMSO-d_6$. 1H and ^{13}C chemical shifts were reported in ppm (δ) relative to internal TMS (δ_H 0.00 ppm). Additionally, data from 2D-NMR experiments COSY, HSQC and HMBC were used to get the unambiguous assignment of the signals and thus the structural characterization of the ligands. HRMS were obtained by LC/MSD TOF on an Agilent Technologies instrument with ESI as ionization source using DMSO as solvent. Electronic absorption spectra of DMSO solutions were recorded on a HP/Agilent 8453 UV-Visible spectrophotometer with a HP/Agilent 89090A Peltier Temperature Controller. EPR spectra of powder samples and DMSO solutions were performed under no-saturation conditions on a Bruker Elexsys E-500 spectrometer using the X-band (9.8 GHz) with 100 kHz modulation frequency. Measurements at room temperature (295 K) of powder samples were recorded in 4 mm O.D. quartz EPR tubes while fluid DMSO solutions in a 1 mm I.D. flat cell. Determinations at 77 K were obtained with frozen DMSO solutions using liquid nitrogen. The *g*- and *A*-values were calculated using the microwave frequency and measuring the magnetic field and confirmed by computer simulation with easyspin computational package in Matlab [11], the instructions outlined above do not include second order corrections. Elemental analyses were carried out on a Perkin Elmer 2400 Series II CHNS/O analyzer using cysteine as internal standard. Magnetic susceptibility measurements at room temperature of powder samples were performed on a Sherwood Scientific Magnetic Susceptibility Balance using the Gouy method. Melting points were measured in sealed capillaries on a Stuart SMP10/120 V/60 digital melting point apparatus with three-digit LED display and are uncorrected.

2.3. X-ray crystallographic structure determinations

Crystals of complexes 6–8 mounted on a glass fiber were studied with an Oxford Diffraction Gemini “A” diffractometer with a CCD area

detector ($\lambda_{MoK\alpha} = 0.71073\text{ \AA}$, monochromator: graphite) source equipped with a sealed X-ray source tube at 130 K.

Unit cell constants were determined with a set of 15/3 narrow frame/runs (1° in ω) scans. A data set consisted of 1054, 528 and 856 frames of intensity collected for 6–8, respectively, with a frame width of 1° in ω , a counting time of 7 s/frame, and a crystal-to-detector distance of 55.00 mm. The double pass method of scanning was used to exclude any noise. The collected frames were integrated by using an orientation matrix determined from the narrow frame scans. CrysAlisPro and CrysAlis RED software packages [12] were used for data collection and integration. Analysis of the integrated data did not reveal any decay. Final cell constants were determined by a global refinement of 17744, 5160 and 4166 reflections ($\theta < 26.3^\circ$) for 6–8, respectively. Collected data were corrected for absorbance by using analytical numeric absorption correction [12a] using a multifaceted crystal model based on expressions upon the Laue symmetry using equivalent reflections. Structure solution and refinement were carried out with the SHELXS-2014 [12b] and SHELXL-2014 [12c]. WinGX v2014.1 software was used to prepare material for publication [12d]. Full-matrix least-squares refinement was carried out by minimising $(Fo^2 - Fc^2)^2$. All non-hydrogen atoms were refined anisotropically. H atoms of the hydroxy and water groups (H–O) were located at a difference map and refined isotropically with $Uiso(H) = 1.5$ for H–O. H atoms attached to carbon were placed in geometrically idealized positions and refined as riding on their parent atoms, with $C-H = 0.95\text{--}0.99\text{ \AA}$ and with $Uiso(H) = 1.2Ueq(C)$ for aromatic and methylene groups, and $Uiso(H) = 1.5Ueq(C)$ for methyl groups.

Details of the X-ray studies for compounds 6–8 are summarized in Table 1 and selected bond lengths and angles parameters are listed in Table 2. Crystallographic data have been deposited at the Cambridge Crystallographic Data Center as Supplementary material number CCDC 1822762 (6), 1589634 (7) and 1589635 (8). Copies of the data can be obtained free of charge on application to CCDC, 12 Union Road, Cambridge CB2 1EZ, UK. e-mail: deposit@ccdc.cam.ac.uk.

2.4. Cytotoxic activity

Human tumor (HeLa, cervix; HCT-15, colorectal) cell lines were purchased from American Type Culture Collection (ATCC). HeLa was propagated in Eagle's Minimum Essential Medium (EMEM; ATCC) and HCT-15 in Roswell Park Memorial Institute Medium (RPMI; Gibco, Invitrogen corporation). In both cases, the cell culture media was supplemented with 10% fetal bovine serum (FBS; Gibco, Invitrogen corporation) without antibiotics.

Experiments were performed with cells within at least five passages from each other. All cells were split when 70–80% confluence was reached using 0.25% trypsin-PBS. Briefly, 2×10^4 cells/well were plated in 96-well microplates with 100 μL of medium supplemented with 10% FBS and allowed to attach, incubating at 37°C and 5% CO_2 for 24 h. At the end of the incubation period, the medium was aspirated and the cells were exposed to coordination compounds in six different concentrations (1000, 100, 10, 1, 0.1 and 0.01 $\mu\text{g/mL}$) for 24 h under conditions previously described. The solutions of the compounds were obtained by preparing a 10 mg/mL stock solution in DMSO followed by decimal serial dilutions with propylene glycol. Cisplatin was used as drug control. An important consideration is that compound 8 was not evaluated at 1000 $\mu\text{g/mL}$ but 500 $\mu\text{g/mL}$ as highest concentration due to its solubility.

Cell growth was determined according to the sulforhodamine B (SRB) assay [13]. *In vitro* studies were done in triplicate and data are expressed as mean \pm SE. Absorbance was measured at 490 nm in a Daigger model ELx800 microplate reader and % cell growth of each concentration of each compound was calculated as: % growth = $100 \times [T/C]$; being T the optical density of the treated wells and C is the optical density of untreated wells. The concentration that induces 50% of maximum inhibition of cell proliferation (IC_{50}) was

Table 1
Crystal data and structure refinement parameters of complexes 6–8.

Identification code	6	7	8
Empirical formula	C ₂₀ H ₁₄ N ₂ O ₃ V	C ₂₄ H ₂₆ N ₂ O ₇ V	C ₂₂ H ₂₀ N ₂ O ₆ V
Formula weight	381.27	505.41	459.34
Crystal system	Monoclinic	Triclinic	Triclinic
Space group	C 2/c	P -1	P -1
Temperature (K)	130(2)	130(2)	130(2)
Wavelength (Å)	0.71073	0.71073	0.71073
Unit cell dimensions			
a (Å)	27.2851(9)	8.3396(6)	7.4958(7)
b (Å)	6.9278(2)	11.5493(12)	11.1969(11)
c (Å)	39.5380(15)	12.9875(11)	12.3066(8)
α (°)	90	100.558(8)	72.646(7)
β (°)	106.108(4)	107.175(7)	89.869(7)
γ (°)	90	96.368(7)	79.019(8)
Volume (Å ³)	7180.3(4)	1156.62(18)	966.18(15)
Z	16	2	2
ρ _{calc} (g cm ⁻³)	1.411	1.451	1.579
μ (mm ⁻¹)	0.574	0.477	0.559
F (0 0 0)	3120	526	474
Crystal size (mm)	0.40 × 0.36 × 0.28	0.42 × 0.33 × 0.28	0.37 × 0.14 × 0.05
θ range (°)	3.541–25.681	3.372–25.680	3.429–30.143
Index ranges	–32 ≤ h ≤ 32 –8 ≤ k ≤ 8 –47 ≤ l ≤ 47	–10 ≤ h ≤ 10 –14 ≤ k ≤ 14 –15 ≤ l ≤ 15	–10 ≤ h ≤ 10 –14 ≤ k ≤ 15 –16 ≤ l ≤ 17
Reflections collected	80463	22,717	13,883
Independent reflections [R _{int}]	6562 [0.0669]	4374 [0.0721]	4947 [0.0351]
Completeness to θ = 26.3°	99.7%	99.8%	99.7%
Data/restraints/parameters	6562/0/469	4374/0/337	4947/0/285
Goodness-of-fit on F ²	1.242	1.244	1.058
Final R, wR2 indexes			
I ≥ 2 s (I)	0.0707, 0.1329	0.0594, 0.1592	0.0402, 0.0860
All data	0.0739, 0.1343	0.0815, 0.1814	0.0574, 0.0976
Δρ Maximum (eÅ ⁻³)	0.540	1.130	0.356
Δρ Minimum (eÅ ⁻³)	–0.567	–0.542	–0.378

Refinement method: Full-matrix least-squares on F².

Table 2
Selected bond lengths (Å) and bond angles (°) for compounds 6–8.

Bond	6 ^a	7	8
N(1)-V(1)/N(3)-V(2)	2.056(4)/2.062(4)	2.056(3)	2.059(1)
N(2)-V(1)/N(4)-V(2)	2.072(3)/2.076(3)	2.052(2)	2.051(2)
O(1)-V(1)/O(4)-V(2)	1.922(3)/1.927(3)	1.925(2)	1.926(2)
O(2)-V(1)/O(5)-V(2)	1.925(3)/1.930(3)	1.918(2)	1.930(1)
O(3)-V(1)/O(6)-V(2)	1.596(3)/1.601(3)	1.609(3)	1.617(1)
O(3)-V(1)-O(1)/O(6)-V(2)-O(4)	110.5(1)/110.2(1)	107.8(1)	109.78(6)
O(3)-V(1)-O(2)/O(6)-V(2)-O(5)	108.2(1)/108.4(1)	107.5(1)	109.61(7)
O(1)-V(1)-O(2)/O(4)-V(2)-O(5)	86.3(1)/85.8(1)	86.1(1)	83.54(6)
O(3)-V(1)-N(2)/O(6)-V(2)-N(4)	103.5(1)/104.9(1)	103.8(1)	105.98(7)
O(1)-V(1)-N(2)/O(4)-V(2)-N(4)	145.7(1)/144.7(1)	88.0(1)	144.04(6)
O(2)-V(1)-N(2)/O(5)-V(2)-N(4)	87.5(1)/87.4(1)	148.5(1)	88.17(6)
O(3)-V(1)-N(1)/O(6)-V(2)-N(3)	105.9(1)/105.9(1)	108.8(1)	106.65(7)
O(1)-V(1)-N(1)/O(4)-V(2)-N(3)	87.8(1)/87.4(1)	142.9(1)	87.95(6)
O(2)-V(1)-N(1)/O(5)-V(2)-N(3)	145.3(1)/145.2(1)	87.9(1)	143.53(6)
N(2)-V(1)-N(1)/N(4)-V(2)-N(3)	78.6(1)/78.4(1)	78.5(1)	78.25(6)

^a Values are given for the two independent molecules present in the asymmetric unit of the crystal lattice.

determined using DoseResp sigmoidal fitting function in OriginPro 2016 [14] by plotting the percent of cell growth against the Log of the drug concentration. Statistical analysis was performed by one-way ANOVA followed by Dunnett's multiple comparison test using GraphPad Prism 5 software [15].

2.5. Synthesis

2.5.1. Ligands

General procedure. The salphen ligands (1–5) were prepared by the condensation reaction of *o*-phenylenediamine with the respective

aldehyde in a 1:2 molar ratio by adapting a reported procedure [16]. Reagents were dissolved in anhydrous ethanol (50 mL) in a 100 mL flat-bottomed flask, equipped with a reflux condenser and a magnetic stirrer. Reactions were refluxed for 6 h. In all cases a translucent solution was observed. Subsequently, the solid products formed were filtered off while the reaction mixture was still hot, purified with cold anhydrous ethanol (3 × 10 mL) washes and vacuum-dried. Fig. 1 indicates the assigned numbering for ligands characterization.

2.5.1.1. *N,N'*-bis(salicylidene)-*o*-phenylenediamine (1). **Reagents:** 2-Hydroxybenzaldehyde (2.441 g, 20 mmol) and *o*-phenylenediamine (1.080 g, 10 mmol). **Product:** 2.945 g (9.3 mmol) of a yellow powder was obtained after purification. **Yield:** 93%. **Mp:** 166–167 °C. **Anal. Calcd.** for C₂₀H₁₆N₂O₂ (M = 316.4 gmol⁻¹): C, 75.93; H, 5.10; N, 8.86%. **Found:** C, 75.86; H, 5.15; N, 9.11%. **IR** (ATR, ν cm⁻¹): 3053 (C–H)_{arom}, 1610 (C=N), 1584, 1560, 1480 (C=C)_{arom}, 1190 (C–O).

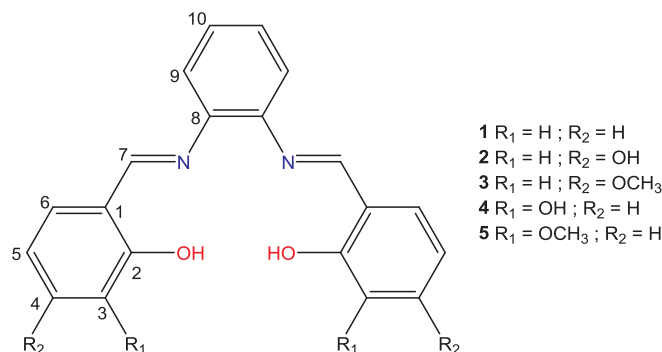


Fig. 1. Chemical structures of the Schiff base ligands employed.

NMR (400 MHz, DMSO- d_6 , 298 K) δ (ppm). ^1H : 6.92–7.01 (m, 4H; H₃, H₅), 7.38–7.48 (m, 6H; H₁₀, H₄, H₉), 7.66 (dd, $J = 8.2, 1.9$ Hz, 2H; H₆), 8.93 (s, 2H; H₇), 12.93 (s, 2H; OH). ^{13}C : 116.64 (C₃), 119.05 (C₅), 119.46 (C₁), 119.72 (C₉), 127.76 (C₁₀), 132.42 (C₆), 133.40 (C₄), 142.23 (C₈), 160.35 (C₂), 164.00 (C₇).

2.5.1.2. *N,N'*-bis(4-hydroxysalicylidene)-*o*-phenylenediamine

(2). **Reagents**: 2,4-Dihydroxybenzaldehyde (2.768 g, 20 mmol) and *o*-phenylenediamine (1.083 g, 10 mmol). **Product**: 2.860 g (8.2 mmol) of a yellow powder was obtained after purification. **Yield**: 82%. **Mp**: 227–228 °C. **Anal. Calcd.** for C₂₀H₁₆N₂O₄ ($M = 348.4$ gmol⁻¹): C, 68.96; H, 4.63; N, 8.04%. **Found**: C, 69.40; H, 4.44; N, 8.3%. **IR** (ATR, ν cm⁻¹): 3327 (O–H), 3057 (C–H)_{arom}, 1608 (C=N), 1575, 1540, 1501, 1452 (C=C)_{arom}, 1188 (C–O). **NMR** (400 MHz, DMSO- d_6 , 298 K) δ (ppm). ^1H : 6.29 (d, $J = 2.3$ Hz, 2H; H₃), 6.39 (dd, $J = 8.5, 2.3$ Hz, 2H; H₅), 7.29–7.34 (m, 2H; H₁₀), 7.35–7.39 (m, 2H; H₉), 7.43 (d, $J = 8.5$ Hz, 2H; H₆), 8.74 (s, 2H; H₇), 10.27 (s, 2H; OH), 13.39 (s, 2H; OH). ^{13}C : 102.41 (C₃), 107.82 (C₅), 112.28 (C₁), 119.47 (C₁₀), 127.01 (C₉), 134.42 (C₆), 142.01 (C₈), 162.63 (C₄), 162.89 (C₇), 163.31 (C₂).

2.5.1.3. *N,N'*-bis(4-methoxysalicylidene)-*o*-phenylenediamine

(3). **Reagents**: 2-Hydroxy-4-methoxybenzaldehyde (3.052 g, 20 mmol) and *o*-phenylenediamine (1.088 g, 10 mmol). **Product**: 3.129 g (8.3 mmol) of a yellow crystalline compound was obtained after purification. **Yield**: 83%. **Mp**: 174–175 °C. **Anal. Calcd.** for C₂₂H₂₀N₂O₄ ($M = 376.4$ gmol⁻¹): C, 70.20; H, 5.36; N, 7.44%. **Found**: C, 69.68; H, 5.26; N, 7.83%. **IR** (ATR, ν cm⁻¹): 3059 (C–H)_{arom}, 1607 (C=N), 1583, 1567, 1509, 1463 (C=C)_{arom}, 1199 (C–O). **NMR** (400 MHz, DMSO- d_6 , 298 K) δ (ppm). ^1H : 3.80 (s, 6H; OCH₃), 6.49 (d, $J = 2.4$ Hz, 2H; H₃), 6.54 (dd, $J = 8.6, 2.5$ Hz, 2H; H₅), 7.32–7.36 (m, 2H; H₉), 7.40–7.43 (m, 2H; H₁₀), 7.54 (d, $J = 8.6$ Hz, 2H; H₆), 8.82 (s, 2H; H₇), 13.51 (s, 2H; OH). ^{13}C : 55.45 (OCH₃), 100.82 (C₃), 106.83 (C₅), 113.16 (C₁), 119.43 (C₁₀), 127.22 (C₉), 134.04 (C₆), 141.69 (C₈), 162.78 (C₇), 163.54 (C₄), 163.82 (C₂).

2.5.1.4. *N,N'*-bis(3-hydroxysalicylidene)-*o*-phenylenediamine

(4). **Reagents**: 2,3-Dihydroxybenzaldehyde (2.770 g, 20 mmol) and *o*-phenylenediamine (1.089 g, 10 mmol). **Product**: 2.931 g (8.4 mmol) of a red–orange crystalline compound was obtained after purification. **Yield**: 84%. **Mp**: 204–206 °C. **Anal. Calcd.** for C₂₀H₁₆N₂O₄ ($M = 348.4$ gmol⁻¹): C, 68.96; H, 4.63; N, 8.04%. **Found**: C, 68.47; H, 4.37; N, 8.07%. **IR** (ATR, ν cm⁻¹): 3463 (O–H), 3051 (C–H)_{arom}, 1617 (C=N), 1580, 1544, 1522, 1467 (C=C)_{arom}, 1208 (C–O). **NMR** (400 MHz, DMSO- d_6 , 298 K) δ (ppm). ^1H : 6.79 (t, $J = 7.8$ Hz, 2H; H₅), 6.95 (dd, $J = 7.9, 1.6$ Hz, 2H; H₄), 7.12 (dd, $J = 7.8, 1.6$ Hz, 2H; H₆), 7.39–7.44 (m, 4H; H₁₀, H₉), 8.88 (s, 2H; H₇); 9.24 (s, 2H; OH), 12.90 (s, 2H; OH). ^{13}C : 118.74 (C₅), 119.11 (C₄), 119.58 (C₁), 119.96 (C₉), 122.77 (C₆), 127.70 (C₁₀), 142.15 (C₈), 145.62 (C₃), 149.45 (C₂), 164.74 (C₇).

2.5.1.5. *N,N'*-bis(3-methoxysalicylidene)-*o*-phenylenediamine

(5). **Reagents**: 2-Hydroxy-3-methoxybenzaldehyde (3.041 g, 20 mmol) and *o*-phenylenediamine (1.080 g, 10 mmol). **Product**: 2.977 g (7.9 mmol) of an orange crystalline compound was obtained after purification. **Yield**: 79%. **Mp**: 172–173 °C. **Anal. Calcd.** for C₂₂H₂₀N₂O₄ ($M = 376.4$ gmol⁻¹): C, 70.20; H, 5.36; N, 7.44%. **Found**: C, 70.88; H, 5.36; N, 7.68%. **IR** (ATR, ν cm⁻¹): 3058 (C–H)_{arom}, 1609 (C=N), 1586, 1568, 1456 (C=C)_{arom}, 1204 (C–O). **NMR** (400 MHz, DMSO- d_6 , 298 K) δ (ppm). ^1H : 3.81 (s, 6H; OCH₃), 6.90 (t, $J = 7.9$ Hz, 2H; H₅), 7.12 (dd, $J = 8.1, 1.4$ Hz, 2H; H₄), 7.25 (dd, $J = 7.9, 1.5$ Hz, 2H; H₆), 7.38–7.42 (m, 2H; H₁₀), 7.44–7.47 (m, 2H; H₉), 8.92 (s, 2H; H₇), 13.00 (s, 2H; OH). ^{13}C : 55.65 (OCH₃), 115.42 (C₄), 118.53 (C₅), 119.32 (C₁), 119.78 (C₉), 123.76 (C₆), 127.78 (C₁₀), 142.08 (C₈), 147.86 (C₃), 150.60 (C₂), 164.29 (C₇).

2.5.2. Vanadium complexes

General procedure. VO(acac)₂ was added carefully in small portions to a suspension of the appropriate ligand (1–5) in anhydrous ethanol (50 mL) in a 1:1.1 molar ratio. An excess of ligand in each reaction was used to ensure its maximum complexation. Reactions were magnetic stirred for 24 h at RT in a 100 mL flat-bottomed flask. Reaction media color changed from the ligand suspension color (yellow or orange) to green (6–8) or khaki (9–10). The change of color was very fast in all cases yielding a turbid reaction media. The solid products formed were filtered off, purified with cold anhydrous ethanol (3 × 10 mL) washes and vacuum-dried. Thereafter, vanadium complexes (6–10) were dried at 100 °C for 24 h. Solubility data indicate the amount of vanadium coordination compound in mg dissolved in a specific volume in μL of DMSO. Sonication was sometimes used to promote an effective dissolution of the complexes.

2.5.2.1. *N,N'*-bis(salicylidene)-*o*-phenylenediamine vanadium(IV) oxide complex (6).

Reagents: VO(acac)₂ (0.713 g, 2.7 mmol) and 1 (0.951 g, 3.0 mmol). **Product**: 0.980 g (2.57 mmol) of a green powder was obtained after purification. **Yield**: 95%. **Mp** > 300 °C. **Solubility**: soluble 1 in 100 parts of DMSO at 25 °C. **Anal. Calcd.** for VO (C₂₀H₁₄N₂O₂) ($M = 381.3$ gmol⁻¹): C, 63.00; H, 3.70; N, 7.35%. **Found**: C, 62.84; H, 3.39; N, 7.49%. **IR** (ATR, ν cm⁻¹): 3048 (C–H)_{arom}, 1601 (C=N), 1577, 1531, 1459 (C=C)_{arom}, 1190 (C–O), 981 (V=O). μ_{eff} 0.87 BM. **TOF⁺** m/z calcd. For (M+H)⁺: 382.3. Found: 382.1. **UV/Vis** (DMSO) λ (nm): 317, 399. Crystals were obtained by vapor diffusion in acetone as solvent and ethanol as precipitant at RT.

2.5.2.2. *N,N'*-bis(4-hydroxysalicylidene)-*o*-phenylenediamine vanadium(IV) oxide complex (7).

Reagents: VO(acac)₂ (0.717 g, 2.7 mmol) and 2 (1.051 g, 3.0 mmol). **Product**: 0.945 g (2.29 mmol) of a green powder was obtained after purification. **Yield**: 85%. **Mp** > 300 °C. **Solubility**: soluble 1 in 75 parts of DMSO at 25 °C. **Anal. Calcd.** for VO (C₂₀H₁₄N₂O₄) ($M = 413.3$ gmol⁻¹): C, 58.12; H, 3.41; N, 6.79%. **Found**: C, 57.35; H, 3.28; N, 6.79%. **IR** (ATR, ν cm⁻¹): 3315 (O–H), 3062 (C–H)_{arom}, 1597 (C=N), 1577, 1536, 1481, 1422 (C=C)_{arom}, 1121 (C–O), 985 (V=O). μ_{eff} 0.87 BM. **TOF⁺** m/z calcd. for (M+H)⁺: 414.3. Found: 414.0. **UV/Vis** (DMSO) λ (nm): 331, 398. Crystals were obtained by vapor diffusion in acetone as solvent and ethanol as precipitant at RT.

2.5.2.3. *N,N'*-bis(4-methoxysalicylidene)-*o*-phenylenediamine vanadium(IV) oxide complex (8).

Reagents: VO(acac)₂ (0.716 g, 2.7 mmol) and 3 (1.133 g, 3.0 mmol). **Product**: 1.006 g (2.28 mmol) of a green powder was obtained after purification. **Yield**: 84%. **Mp** > 300 °C. **Solubility**: soluble 1 in 200 parts of DMSO at 25 °C. **Anal. Calcd.** for VO (C₂₂H₁₈N₂O₄) ($M = 441.3$ gmol⁻¹): C, 59.87; H, 4.11; N, 6.34%. **Found**: C, 59.96; H, 3.91; N, 6.64%. **IR** (ATR, ν cm⁻¹): 3021 (C–H)_{arom}, 1596 (C=N), 1574, 1521, 1490, 1455 (C=C)_{arom}, 1200 (C–O), 979 (V=O). μ_{eff} 0.85 BM. **TOF⁺** m/z calcd. for (M+H)⁺: 442.3. Found: 442.1. **UV/Vis** (DMSO) λ (nm): 326, 393. Crystals were obtained by slow solvent evaporation in CH₃CN at RT.

2.5.2.4. *N,N'*-bis(3-hydroxysalicylidene)-*o*-phenylenediamine vanadium(IV) oxide complex (9).

Reagents: VO(acac)₂ (0.718 g, 2.7 mmol) and 4 (1.049 g, 3.0 mmol). **Product**: 1.037 g (2.51 mmol) of a khaki powder was obtained after purification. **Yield**: 90%. **Mp** > 300 °C. **Solubility**: soluble 1 in 75 parts of DMSO at 25 °C. **Anal. Calcd.** for VO (C₂₀H₁₄N₂O₄) ($M = 413.3$ gmol⁻¹): C, 58.12; H, 3.41; N, 6.79%. **Found**: C, 57.82; H, 3.03; N, 6.99%. **IR** (ATR, ν cm⁻¹): 3393 (O–H), 3038 (C–H)_{arom}, 1598 (C=N), 1548, 1491, 1442, 1404 (C=C)_{arom}, 1197 (C–O), 972 (V=O). μ_{eff} 0.86 BM. **TOF⁺** m/z calcd. for (M+H)⁺: 414.3. Found: 414.0. **UV/Vis** (DMSO) λ (nm): 334, 351, 430.

2.5.2.5. *N,N'*-bis(3-methoxysalicylidene)-*o*-phenylenediamine vanadium (IV) oxide complex (**10**). **Reagents:** VO(acac)₂ (0.712 g, 2.7 mmol) and **5** (1.131 g, 3.0 mmol). **Product:** 1.080 g (2.45 mmol) of a khaki powder was obtained after purification. **Yield:** 91%. **Mp** > 300 °C. **Solubility:** soluble 1 in 75 parts of DMSO at 25 °C. **Anal. Calcd.** for VO (C₂₂H₁₈N₂O₄) (M = 441.3 gmol⁻¹): C, 59.87; H, 4.11; N, 6.34%. **Found:** C, 59.81; H, 3.82; N, 6.68%. **IR** (ATR, ν cm⁻¹): 3049 (C–H)_{arom}, 1603 (C=N), 1580, 1544, 1434 (C=C)_{arom}, 1204 (C–O), 977 (V=O). μ_{eff} 0.89 BM. **TOF⁺ m/z** calcd. for (M+H)⁺: 442.3. **Found:** 442.1. **UV/Vis** (DMSO) λ (nm): 329, 352, 425.

3. Results and discussion

3.1. General

Ligands **1–5** were obtained with high yield and purity. Additionally, ligands characterization results were highly consistent and in good agreement with previously reported data [16–21]. For vanadium coordination compounds (**6–10**) the Schiff bases acted as tetradentate ligands and coordinated to vanadium(IV) to give a stoichiometric ratio of 1:1 [M:L]. Complexes **7–10**, as well as, their characterization, are reported for their first time; **6** had been previously reported [10,22–25] and the characterization results obtained for this complex were also consistent with the report, except for the effective magnetic moment [22]. Complexes **6–10** were poorly soluble in common organic and inorganic solvents except in DMSO but was possible to solubilize them in water by using the cosolvency technique with propylene glycol as cosolvent. In addition, coordination compounds were stable in air, DMSO and DMSO-Propylene glycol–water solution.

Chemical stability of coordination compounds **6–10** was investigated by UV/Vis spectroscopy. First, stability studies of the complexes in DMSO (c.a. 2.5×10^{-2} M) at 37 °C for 72 h were carried out to determine possible structural changes, such as ligand substitution processes leading to the well-known [VO(DMSO)₂] (absorption bands at 830 and 690 nm) [26]. Such bands were not observed during the study. Subsequently, stability in DMSO-propylene glycol–water (1:9:90) was investigated to verify that coordination compounds were stable under incubation conditions for the *in vitro* studies. The electronic absorption spectra of compounds **6–10** remained unchanged for 72 h at 37 °C. These results allowed to continue with the biological tests.

3.2. Infrared spectroscopy

The infrared spectra of ligands **1–5** exhibited bands at 1607–1617 cm⁻¹ corresponding to ν (C=N) stretching mode [27]. These bands shifted toward lower wavenumbers (1596–1603 cm⁻¹) in the complexes spectra indicating vanadium imine coordination [28].

[V^{IV}O]²⁺ complexes exhibit the IR band associated to the stretching of the (V=O) group in the region of 995–940 cm⁻¹ [29]. According to the literature, this band for the square-pyramidal oxidovanadium(IV) complexes appears at higher wave numbers (995–960 cm⁻¹), while for octahedral [V^{IV}O]²⁺ complexes emerges at 960–940 cm⁻¹ [29]. In the IR spectra of complexes **6–10**, the IR band assigned to the stretching vibration of the (V=O) group was observed at 985–970 cm⁻¹. These observations indicated the square-pyramidal molecular geometry of the complexes.

3.3. Crystal structures

Single crystal X-ray analysis of complexes **6–8** as dark brown (**7**) and dark green (**6**, **8**) blocks, showed similar neutral complexes of the form [VO(L)], exhibiting a metal oxidation state of +4. The basal square plane was constituted by the *N,N'*-bis(salicylidene)-*o*-phenylenediamine molecule for **6**, *N,N'*-bis(4-hydroxysalicylidene)-*o*-phenylenediamine molecule for **7** and *N,N'*-bis(4-methoxysalicylidene)-*o*-phenylenediamine molecule for **8**. In all solid-state structures, the salphen

derivative acted as a tetradentate ligand through its *o*-phenylenediamine N atoms and its deprotonated phenol O atoms. The metal coordination implied the formation of a system of six fused cycles; five of them were six-membered rings and one was a five-membered ring. Displacement ellipsoids plot of **6**, **7** and **8** are shown in Figs. 2, 5 and 8, respectively.

In relation to oxidovanadium(IV) complexes, a new monoclinic (C 2/c; Z = 16) polymorph of compound **6** was obtained. Previously, a monoclinic polymorph (P2(1)/c; Z = 8) of **6** was reported by Tshentu [25]. There are two crystallographically independent molecules in the asymmetric unit of compound **6**, Fig. 2. The structure analysis of **6** showed a square-pyramidal geometry with the vanadium atom lying at 0.585 Å above the mean plane defined by atoms N1/N2/O1/O2 (molecule B) and 0.597 Å for molecule A (N3/N4/O4/O5 plane). The N(1)N(2)O(1)O(2) and N(3)N(4)O(4)O(5) planes from the two molecules bisect each other at an angle of 81.01°. The geometric parameter (τ) of 0.0067 (B) and 0.0083 (A) confirmed a perfectly square-pyramidal geometry [30] for both molecules in complex **6**.

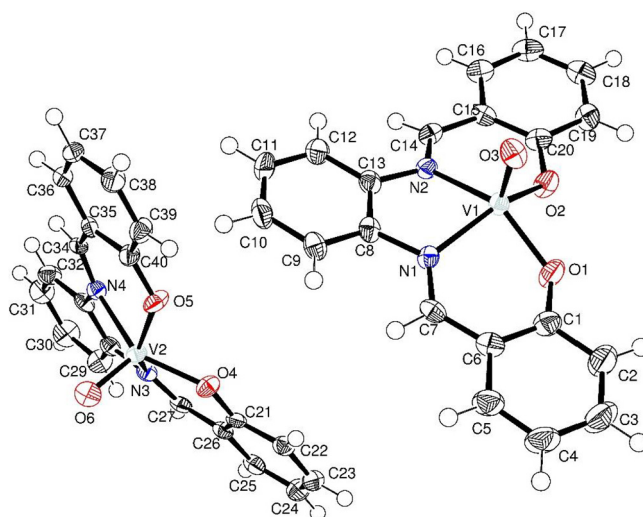


Fig. 2. A perspective view of two molecules, A (left) and B (right), of complex **6** with the atomic labelling scheme. Displacement ellipsoids are shown at the 70% probability level.

In complex **6**, molecules A formed centrosymmetric dimers stabilized by π ... π stacking interactions (3.549 Å). The bilayers formed by these centrosymmetric dimers were also stabilized by π contacts (3.636 Å), Fig. 3.

On the other hand, molecules B of complex **6** were found stacked in monolayers with short π contacts of 3.636 Å, Fig. 4.

Complex **7** consisted of one unit of neutral *N,N'*-bis(4-hydroxysalicylidene)-*o*-phenylenediamine oxidovanadium(IV) compound and two ethanol solvent molecules, Fig. 5. The vanadium atom in **7** is pentacoordinate and is located at 0.580 Å above the mean plane defined by atoms N1/N2/O1/O2. The structural index parameter (τ) of 0.093 evidenced a slightly distorted square-pyramidal geometry [30].

In complex **7**, the molecules formed centrosymmetric dimers by a wide π interaction (3.418 Å) between two cycles of each molecule which also involved the vanadium atom with short distances to the C16 = C17 double bond of the second molecule (C16...V 3.677 and C17...V 3.680 Å; $\Sigma r_{\text{vdw}} = 3.7$ Å). This C16 = C17 bond occupied the sixth coordinative position of vanadium, Fig. 6.

In addition, centrosymmetric dimers formed bilayers which in turn were bound together by hydrogen bonds of the phenol protons with the V = O oxygen atom (O5–H5D...O3V 1.947 Å), Fig. 7.

The asymmetric unit of **8** consisted of a monomeric vanadium(IV) complex, co-crystallized with one equivalent of water solvent molecule in the triclinic *P*-1 space group, Fig. 8. The metal center atom is

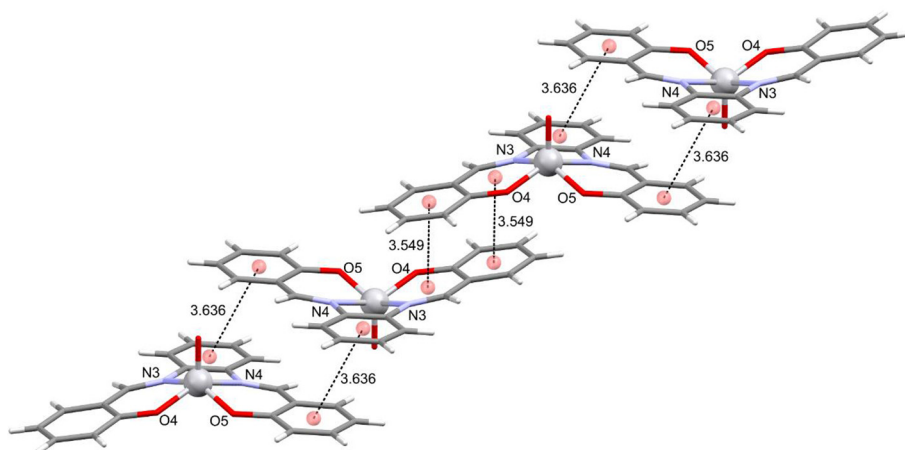


Fig. 3. Centrosymmetric dimers and bilayers formed by molecules A in the crystal of compound 6.

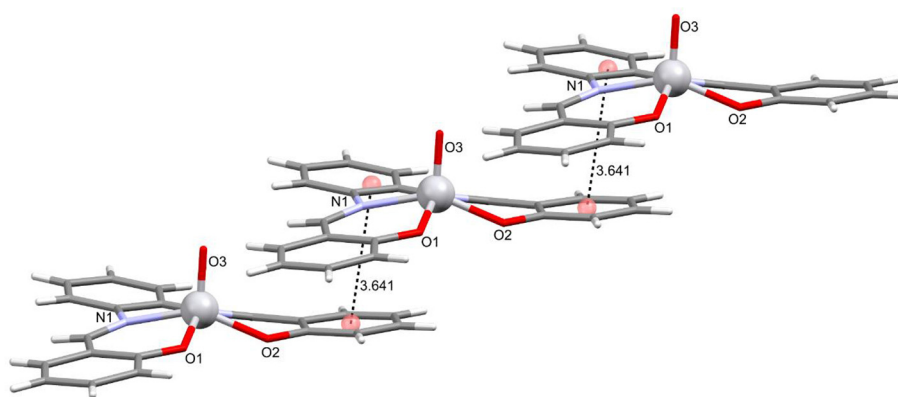


Fig. 4. π -Stacking interactions of molecules B in complex 6.

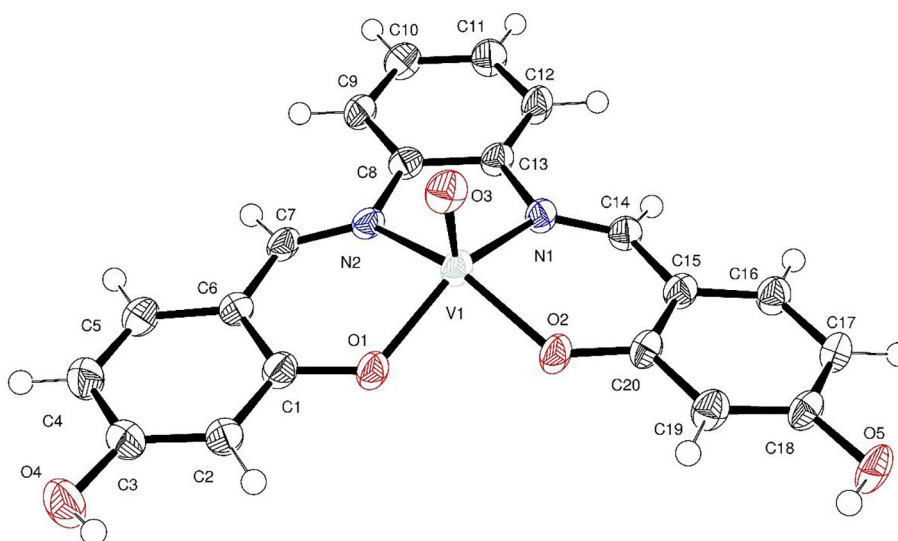


Fig. 5. A perspective view of complex 7 with the atomic labelling scheme. Displacement ellipsoids are shown at the 70% probability level. The ethanol solvent molecules were omitted for clarity.

pentacoordinate and the metrics of the molecule V–N bonds of 2.055(4) Å, V–O bonds of 1.928(2) Å, and a V = O bond of 1.617(1) Å were similar to the current 127 oxidovanadium(2+)-salen complexes found in the Cambridge Structural Database (CDS: ConQuest Version 1.19, [31]). Average literature values for these types of bonds are 2.058,

1.922, and 1.595 Å, respectively. Vanadium atom is located at 0.616 Å above the mean plane defined by atoms N1/N2/O1/O2. The τ parameter of 0.0085 for this compound indicated a purely square-pyramidal geometry [30] for complex 8.

Compound 8 also formed centrosymmetric dimers and were

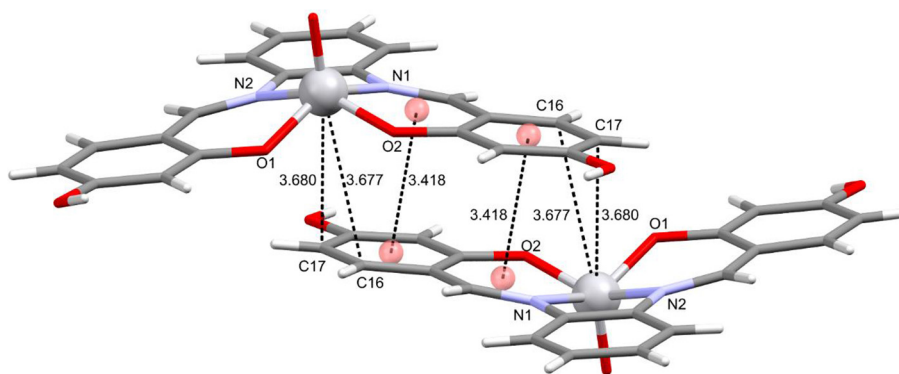


Fig. 6. Centrosymmetric dimer found at the crystal of compound 7.

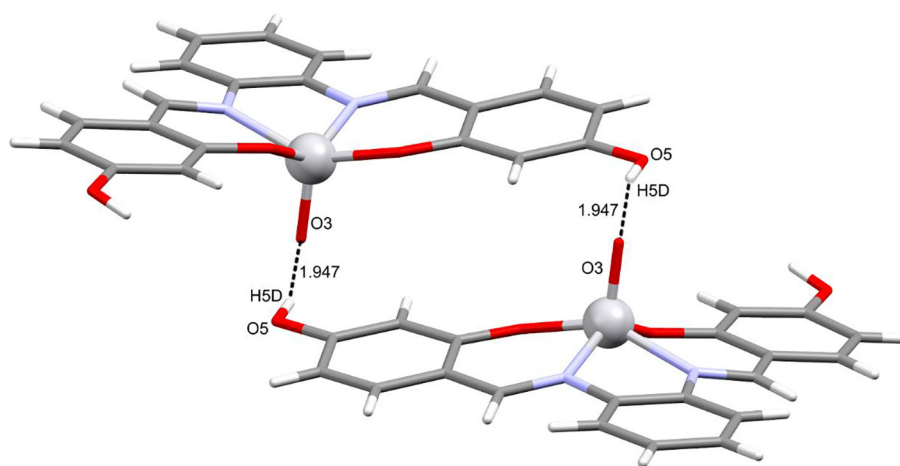


Fig. 7. Hydrogen bonds of the phenol protons with the V = O oxygen atom observed in the bilayers formed by centrosymmetric dimers of compound 7.

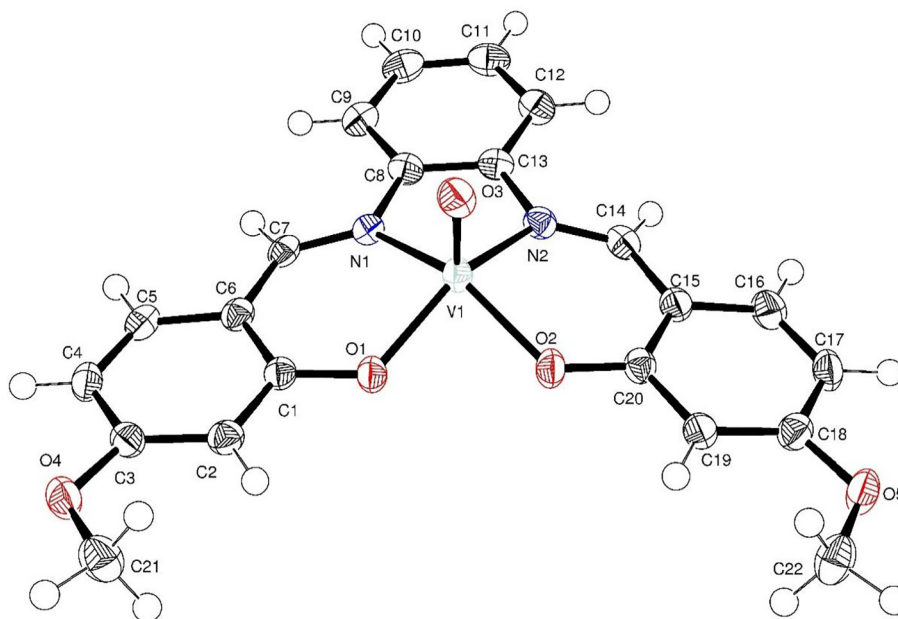


Fig. 8. A perspective view of complex 8 with the atomic labelling scheme. Displacement ellipsoids are shown at the 60% probability level. The water solvent molecule was omitted for clarity.

arranged in two different layers formed by π contacts (3.737 Å) and water hydrogen bonds as is shown in Figs. 9 and 10, respectively.

In the crystal array, intermolecular interactions of O–H...O

hydrogen bonds between the coordinated oxygen atoms and the water molecule were evident: O1W–H1D...O1 (2.177 Å), O1W–H1E...O5 (2.141 Å) and O1W–H1D...O2 (2.501 Å).

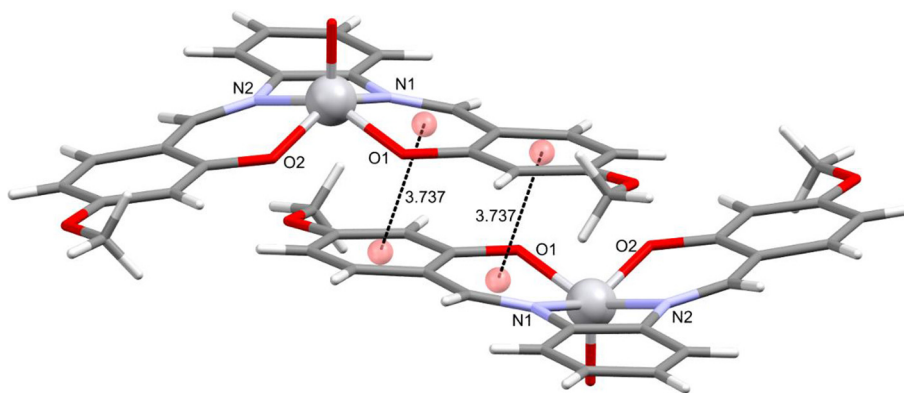


Fig. 9. Centrosymmetric dimer found at the crystal of compound **8**.

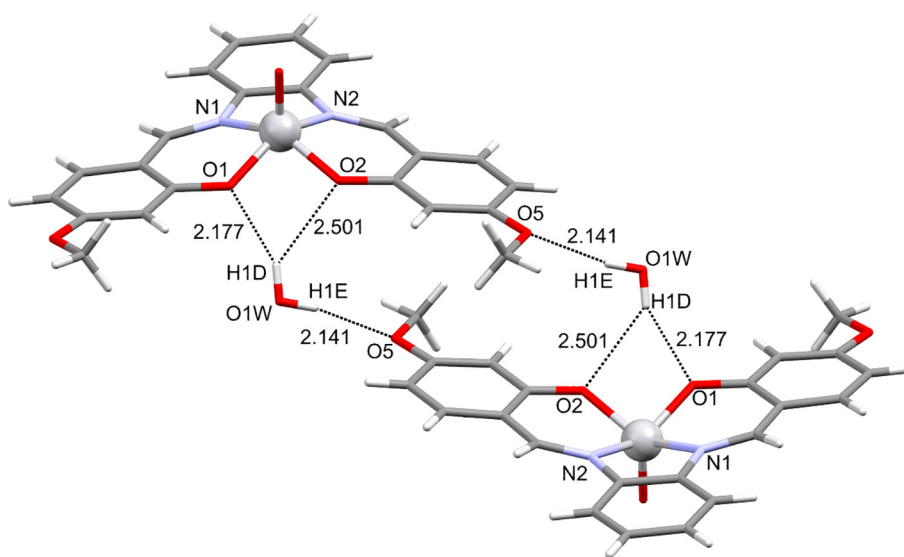


Fig. 10. Centrosymmetric dimers of compound **8** formed bilayers which in turn were also stabilized by water hydrogen bonds.

3.4. Magnetic studies

Effective magnetic moments (μ_{eff}) for vanadium coordination compounds **6–10** were in the range 0.85–0.89 BM. According to the literature, the μ_{eff} for $[\text{V}^{\text{IV}}\text{O}]^{2+}$ complexes range from 1.7 to 1.8 BM which correspond to a single electron of the $3d^1$ system of square-pyramidal oxido vanadium(IV) [32]. Since the spin–orbit coupling for $[\text{V}^{\text{IV}}\text{O}]^{2+}$ complexes is positive [33,34], magnetically dilute oxido vanadium(IV) complexes should display μ_{eff} close to the spin-only magnetic moment of 1.73 BM [35]. Considering that magnetic susceptibility measurements of the complexes **6–10** were obtained at room temperature using the Gouy method without a previous magnetic dilution, the low μ_{eff} may arise from antiferromagnetic spin–spin interaction between the neighboring V^{IV} centers [36] or through a polymeric arrangement [37]. The X-ray crystal structures allowed to discard the two previous explanations.

It is important to emphasize that although the μ_{eff} reported by Kolawole [22] for complex **6** agrees with the expected value, the *in-situ* synthesis strategy, the reagents employed, as well as, the purification techniques carried out by Kolawole, differ considerably from those used by us. Additionally, they did not obtain an X-ray crystal structure. On the other hand, in the paper by Tshentu [25], the μ_{eff} was not determined and the X-ray crystal structure crystallized in a different space group from the one reported herein. For these reasons, we suggest that the low μ_{eff} value obtained for compound **6** maybe due to the short π contacts observed in the centrosymmetric dimers and the bilayers

formed by molecules **A**, as well as, the monolayer found at molecules **B** also stabilized by π interactions. For complexes **7** and **8** the subnormal μ_{eff} maybe due to the existing intermolecular interactions; in both cases to the presence of centrosymmetric dimers stabilized by wide π interactions and by hydrogen bonds (in the case of compounds **9** and **10** we propose a similar behavior). In addition, all samples were magnetically concentrated because the solid state EPR spectra (X-band) at room temperature consisted of only one wide isotropic signal with g -values close to 1.990 (Table 3).

The EPR spectrum of $[\text{VO}(\text{salphen})]\cdot\text{MeCN}$ in acetonitrile solution at room temperature has been previously reported by Wang [24,38]. However, they reported a g -value larger than that observed in most $[\text{V}^{\text{IV}}\text{O}]^{2+}$ complexes. Herein, the EPR spectra of oxido vanadium(IV) compounds **6–10** in DMSO solution at room temperature (295 K) displayed a *quasi-isotropic* signal with g -values around 1.97 which was split into eight hyperfine lines due to the spin of ^{51}V nucleus ($I = 7/2$) but an unequal separation of the hyperfine component was observed, Fig. 11. This occurrence could be due to the second-order effect like rotational incipient slow-tumbling of the $\text{V}(\text{IV})$ ion in DMSO solution generating asymmetric absorption line shapes and a wide linewidth [39]. The g -values were very similar in all coordination compounds studied. However, the *quasi-isotropic* A -values showed greater changes, indicating to be more sensitive to the coordination environment of the $[\text{V}^{\text{IV}}\text{O}]^{2+}$ ion as was early reported by Pecoraro [40] and Liboiron [41]. EPR parameters for complexes **6–10** in fluid DMSO solution at RT are collected in Table 3.

Table 3

Best fit EPR parameters of complexes **6–10**. Hyperfine coupling constants (A) are given in units of 10^{-4} cm^{-1} and the pick-to-pick first-derivative linewidth (ΔB_{pp}) in units of Gauss.

Compound	RT (298 K)				LN (77 K)				
	Solid state		DMSO solution		Frozen DMSO solution				
	g	ΔB_{pp}	g	A	$g_{ }$	g_{\perp}	g_{aver}	$A_{ }$	A_{\perp}
6	1.987	98	1.976	87	1.956	1.975	1.969	160	54
7	1.994	138	1.978	81	1.956	1.975	1.969	160	56
8	1.996	85	1.976	85	1.956	1.976	1.970	160	54
9	1.980	53	1.977	85	1.959	1.986	1.977	160	56
10	1.992	184	1.975	85	1.959	1.976	1.971	160	54

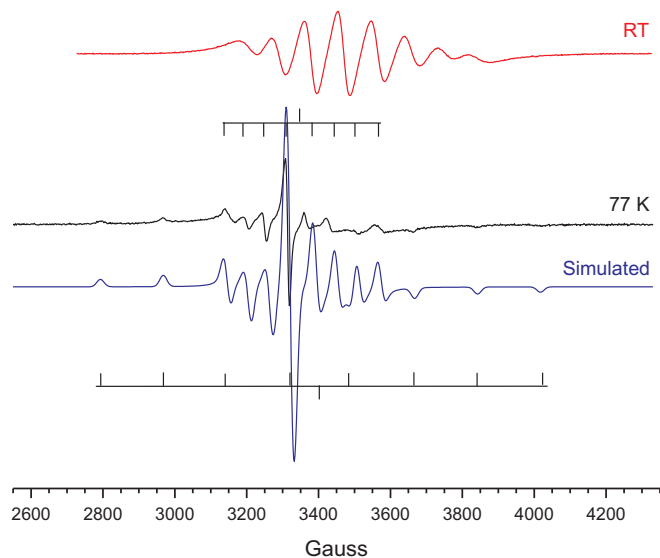


Fig. 11. X-band EPR spectra of **9** in DMSO solution recorded at room temperature (top), in frozen DMSO solution at 77 K (middle) and simulated (bottom).

The X-band EPR spectra of frozen DMSO solutions for complexes **6–10** showed typical axial spectra with two sets of eight lines each (Fig. 11), indicating an equatorial binding mode. The best fit EPR parameters are compiled in Table 3. In all cases, $g_{||}$ -values were very similar among them and $g_{average}$ -values were around 1.97. A -values were $160 \times 10^{-4} \text{ cm}^{-1}$ for the parallel component ($A_{||}$) and around $56 \times 10^{-4} \text{ cm}^{-1}$ for the perpendicular component (A_{\perp}). The latter were slightly higher than the reported values for other oxidovanadium (IV) salen-type complexes [25,42–43]. Vanadium complexes **6–10** exhibited a similar coordination sphere by the N_2O_2 donor group of the salphen ligand in the equatorial plane, for this reason the $A_{||}$ did not show great changes and resulted in $160 \times 10^{-4} \text{ cm}^{-1}$. Likewise, A_{\perp} -values showed small changes in line position, mainly for compounds **6**, **8** and **10** which displayed the lowest A_{\perp} -value while complexes **7** and **9** the highest. This suggested a higher electron density over the V(IV) atom in compounds **7** and **9** due to the contribution of the salphen-type ligand employed in each case. The effect of the contribution of donor group to the hyperfine coupling in V(IV) complexes has been already reported [36,37].

3.5. Cytotoxicity

Cytotoxic activity results of complexes **6–10** on human cancer (HeLa and HCT-15) cell lines after 24 h of exposition are summarized in Table 4 and Fig. 12. Cisplatin is included for comparison. The IC_{50} value indicates the concentration required to inhibit 50% of the cancer cell growth. In the present study, propylene glycol was used as cosolvent in

Table 4

IC_{50} values of complexes **6–10** toward the selected cell lines. ND = Not Determined.

Compound	IC_{50} (μM)	
	HeLa	HCT-15
6	1.502 ± 0.023	1.415 ± 0.009
7	1.075 ± 0.003	ND
8	0.483 ± 0.003	0.373 ± 0.004
9	0.443 ± 0.005	0.875 ± 0.005
10	0.042 ± 0.004	2.122 ± 0.008
Cisplatin	1.200 ± 0.004	2.135 ± 0.010

the 96-well microplates.

Cytotoxic activity in HeLa indicated that complexes **7–10** were more active than the control, complex **6** was not effective enough compared with cisplatin. Statistical analysis revealed that IC_{50} value corresponding to each compound was significantly different from that obtained for the control. By contrast, *in vitro* cytotoxic effect in HCT-15 indicated that all compounds were more active than cisplatin, except complex **7**, for which the IC_{50} was not determined because the percentage of cell survival at $1000 \mu\text{g}/\text{mL}$ exceeded the 50%. Statistical analysis indicated that IC_{50} values corresponding to the complexes prepared were significantly different from the control except for compound **10**, whose IC_{50} value was statistically equal to that observed for cisplatin. The difference previously described is entirely associated with the experiment *per se* (i.e. the effect of treatment on cells) and not by issues related to the experimenter since the assays were performed under the same conditions.

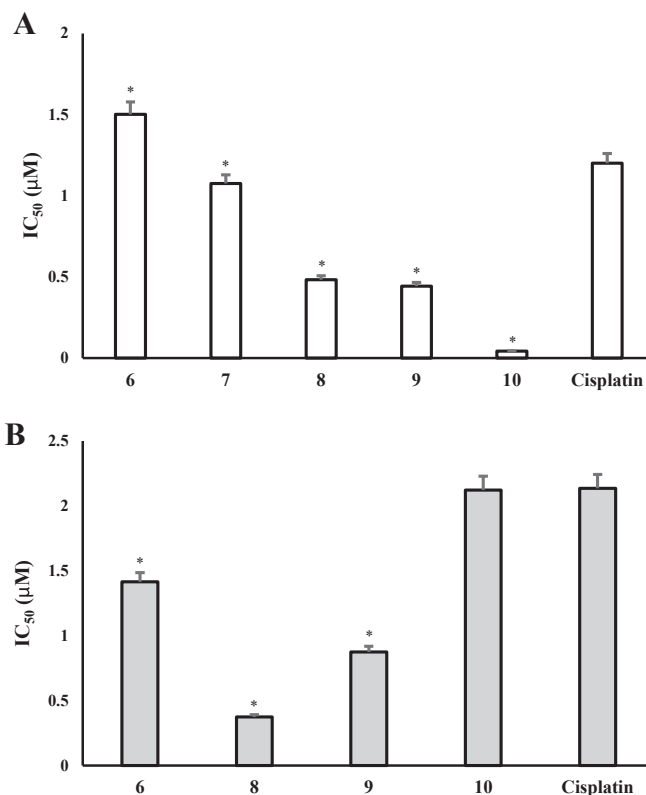


Fig. 12. Cytotoxic effect of complexes **6–10** and cisplatin (control) against HeLa (A) and HCT-15 (B). * = significantly difference with $p < 0.05$. IC_{50} for compound **7** was not possible to determine on HCT-15.

Regardless of the cancer cell line type, compounds **6** and **8** displayed similar IC_{50} values. On the other hand, compound **10** showed larger sensitivity for colorectal cancer. Although this assay cannot give further

insights into the structure-activity relationship, it could be thought that the effect observed by complexes **6** and **8** is due to the complex *per se* and is not influenced by the cancer cell type. Since the antiproliferative and anticancer effects of vanadium compounds have been ascribed to protein tyrosine phosphatases inhibition (e.g., due to phosphate-antagonizing vanadates or peroxovanadium species, formed as possible biotransformation products from $[V^{IV}O]^{2+}$ ions, dependent on pH and redox environment) and the generation of reactive oxygen species (elicited by the complex redox chemistry of vanadium) as the foremost [44–47], the underlying mechanisms continue not to be well understood [3,48].

Complexes whose IC_{50} value is lower than that obtained for cisplatin are promising candidates for further investigations, however, in this study it would be interesting to learn about the effect of the complexes upon a longer exposure time to establish the time of maximum effect and then expand the research to other tumor and healthy cell lines to understand the cytotoxic potential of these oxidovanadium(IV) complexes.

4. Conclusions

In summary, five vanadium coordination compounds (**6–10**) have been synthesized and fully characterized. These vanadium complexes presented an oxidation state of +4. Oxidovanadium(IV) compounds exhibited a square-pyramidal molecular geometry around the $[V^{IV}O]^{2+}$ ion. The X-ray crystal structures revealed that in complexes **6–8** the vanadium atom formed an uncommon, unsaturated planar fused hexacyclic system and we suggest that such arrangement could be the responsible for the anomalous effective magnetic moments values, for complexes **9** and **10** we propose a similar behavior. Finally, cytotoxic effect exhibited *in vitro* for complexes **6** and **8** was similar on both cancer cell types and thus could be an insight into the structure-activity relationship for these types of vanadium coordination compounds.

Acknowledgments

This research was supported by grants from PAIP 50009036 and CONACyT 178851. Authors thank BSc. M. Gutiérrez-Franco, MSc. N. López-Balbiaux and MSc. V. Lemus-Neri for data processing, BSc. P. Fierro-Ramírez for technical support and PhD. Karla P. Salas-Martin for her invaluable help and assistance in the preparation of this manuscript. JHB thanks the support provided by Sub127-DSA-UNAM.

Appendix A. Supplementary data

Supplementary data associated with this article can be found, in the online version, at <http://dx.doi.org/10.1016/j.ica.2018.05.013>.

References

- [1] E. Kioseoglou, S. Petanidis, C. Gabriel, A. Salifoglou, *Coord. Chem. Rev.* 301–302 (2015) 87–105.
- [2] S.K. Panchal, S. Wanyonyi, L. Brown, *Curr Hypertens Rep.* 19 (2017) 10.
- [3] J.C. Pessoa, *J. Inorg. Biochem.* 147 (2015) 4–24.
- [4] J.L. Domingo, M. Gómez, *Food Chem. Toxicol.* 95 (2016) 137–141.
- [5] (a) K. Gruzewska, A. Michno, T. Pawelczyk, H. Bielarczyk, *J. Physiol. Pharmacol.* 65 (2014) 603–611; (b) D.C. Crans, *J. Org. Chem.* 80 (2015) 11899–11915; (c) C.C. McLauchlan, B.J. Peters, G.R. Willsky, D.C. Crans, *Coord. Chem. Rev.* 301–302 (2015) 163–199; (d) D.C. Crans, M.L. Tarlton, C.C. McLauchlan, *Eur. J. Inorg. Chem.* 27 (2014)

- 4450–4468; (e) M. Xie, D. Chen, F. Zhang, G.R. Willsky, D.C. Crans, W. Ding, *J. Inorg. Biochem.* 136 (2014) 47–56.
- [6] D.C. Crans, K.A. Woll, K. Prusinskas, M.D. Johnson, E. Norkus, *Inorg. Chem.* 52 (2013) 12262–12275.
- [7] A. Rajini, M. Nookaraju, N. Venkathathri, I.A.K. Reddy, *Arab. J. Chem.* 10 (2017) S2082–S2089.
- [8] M.J. Hosseini, F. Shaki, M. Ghazi-Khansari, J. Pourahmad, *Metallomics.* 5 (2013) 152–166.
- [9] S.A. Zabin, M. Abdelbaset, *Eur. J. Chem.* 7 (2016) 322–328.
- [10] V.G. Sankareswari, D. Vinod, A. Mahalakshmi, M. Alamelu, G. Kumaresan, R. Ramaraj, S. Rajagopal, *Dalton Trans.* 43 (2014) 3260–3272.
- [11] S. Stoll, A. Schweiger, *J. Magn. Reson.* 178 (2006) 42–55.
- [12] (a) P.R.O. Agilent CrysAlis R.E.D. CrysAlis Agilent Technologies, Yarnton, England, (2013). (b) R.C. Clark, J.S. Reid, *Acta Crystallogr. A.* 51 (1995) 887–897; (c) G.M. Sheldrick, *Acta Crystallogr. A.* 71 (2015) 3–8; (d) G.M. Sheldrick, *Acta Crystallogr. C.* 71 (2015) 3–8; (e) L.J. Farrugia, *J. Appl. Crystallogr.* 32 (1999) 837–838
- [13] P. Skehan, R. Storeng, D. Scudiero, A. Monks, J. McMahon, D. Vistica, J.T. Warren, H. Bokesch, S. Kenney, M.R. Boyd, *J. Natl. Cancer Inst.* 82 (1990) 1107–1112.
- [14] <http://www.originlab.com/>.
- [15] <https://www.graphpad.com/>.
- [16] D. Olea-Román, N. Bélanger-Desmarais, M. Flores-Álamo, C. Bazán, F. Thouin, C. Reber, S.E. Castillo-Blum, *Dalton Trans.* 44 (2015) 17175–17188.
- [17] A. Mobinikhaledi, P.J. Steel, M. Polson, *Synth. React. Inorg. Metal-Org. Nano-Met. Chem.* 39 (2009) 189–192.
- [18] M.S. Singh, A.K. Singh, P. Singh, R. Jain, *Org. Prep. Proced. Int.* 37 (2005) 173–177.
- [19] M. Bazarganipour, M. Salavati-Niasari, *Chem. Eng. J.* 286 (2016) 259–265.
- [20] H. Deng, B. Liu, C. Yang, G. Li, Y. Zhuang, B. Li, X. Zhu, *RSC Adv.* 4 (2014) 62021–62029.
- [21] S. Majumder, S. Pasayat, A.K. Panda, S.P. Dash, S. Roy, A. Biswas, M.E. Varma, B.N. Joshi, E. Garribba, C. Kausar, S.K. Patra, W. Kaminsky, A. Crochet, R. Dinda, *Inorg. Chem.* 56 (2017) 11190–11210.
- [22] G.A. Kolawole, K.S. Patel, A. Earnshaw, *J. Coord. Chem.* 14 (1985) 57–63.
- [23] M.R. Maurya, A. Kumar, M. Ebel, D. Rehder, *Inorg. Chem.* 45 (2006) 5924–5937.
- [24] X. Wang, X.M. Zhang, H.X. Liu, *Polyhedron* 14 (1995) 293–296.
- [25] A.S. Ogunlaja, W. Chidawanyika, E. Antunes, M.A. Fernandes, T. Nyokong, N. Torto, Z.R. Tshentu, *Dalton Trans.* 41 (2012) 13908–13918.
- [26] K. Kaya, Y. Ikeda, H. Fukutomi, *Bull. Chem. Soc. Jpn.* 58 (1985) 2648–2651.
- [27] G. Das, D.B. Shinde, S. Kandambeth, B.P. Biswal, R. Banerjee, *Chem. Commun.* 50 (2014) 12615–12618.
- [28] R.N. Patel, Y.P. Singh, Y. Singh, R.J. Butcher, J.P. Jasinski, *Polyhedron* 133 (2017) 102–109.
- [29] J. Farzanfar, K. Ghasemi, A.R. Rezvani, H.S. Delarami, A. Ebrahimi, H. Hosseinpour, A. Eskandari, H.A. Rudbari, G. Bruno, *J. Inorg. Biochem.* 147 (2015) 54.
- [30] A.W. Addison, T.N. Rao, J. Reedijk, J. Rijn, G.C. Verschoor, *J. Chem. Soc., Dalton Trans.* (1984) 1349–1356.
- [31] F.H. Allen, *Acta Crystallogr. B* 58 (2002) 380–388.
- [32] A.K. Yadava, H.S. Yadav, U.S. Yadav, D.P. Rao, *ISRN Inorgan. Chem.* 2013 (2013) 5.
- [33] A. Syamal, *Coord. Chem. Rev.* 16 (1975) 309–339.
- [34] N. Katsaros, *Trans. Met. Chem.* 7 (1982) 72–74.
- [35] U.B. Gangadharmath, V.K. Revankar, V.B. Mahale, *Spectrochim. Acta A* 58 (2002) 2651–2657.
- [36] S.N. Rao, D.D. Mishra, R.C. Maurya, N.N. Rao, *Polyhedron* 16 (11) (1997) 1825–1829.
- [37] O.M.I. Adly, A. Taha, S.A. Fahmy, *J. Mol. Struct.* 1083 (2015) 450–459.
- [38] X. Wang, X.M. Zhang, H.X. Liu, *Trans. Met. Chem.* 19 (1994) 611–613.
- [39] R.F. Campbell, J.H. Freed, *J. Phys. Chem.* 84 (1980) 2668–2680.
- [40] T.S. Smith II, R. LoBrutto, V.L. Pecoraro, *Coord. Chem. Rev.* 228 (2002) 1–18.
- [41] B.D. Liboiron, In *High Resolution EPR: Applications to Metalloenzymes and Metals in Medicine* (Biological Magnetic Resonance 28), Springer, New York, 2009.
- [42] I. Correia, J.C. Pessoa, M.T. Duarte, M.F. Minas da Piedade, T. Jackush, T. Kiss, M.M.C.A. Castro, C.F.G.C. Geraldes, F. Avencilla, *Eur. J. Inorg. Chem.* (2005) 732–744.
- [43] P. Zabierowski, J. Szklarzewicz, R. Gryboś, B. Modryl, W. Nitek, *Dalton Trans.* 43 (2014) 17044–17053.
- [44] U. Jungwirth, C.R. Kowol, B.K. Keppler, C.G. Hartinger, W. Berger, P. Heffeter, *Antioxid. Redox Signal.* 15 (2011) 1085–1127.
- [45] D. Rehder, *Dalton Trans.* 42 (2013) 11749–11761.
- [46] L. Habala, C. Bartel, G. Giester, M.A. Jakupc, B.K. Keppler, A. Rempel, *J. Inorg. Biochem.* 147 (2015) 147–152.
- [47] J.C. Pessoa, E. Garribba, M.F.A. Santos, T. Santos-Silva, *Coord. Chem. Rev.* 301–302 (2015) 49–86.
- [48] G. Scalsei, I. Correia, J. Benítez, S. Rostán, F. Marques, F. Mendes, A.P. Matos, J.C. Pessoa, D. Gambino, *J. Inorg. Biochem.* 166 (2017) 162–172.